Real-Time Image-Guided Cooperative Robotic Assist Device for Deep Anterior Lamellar Keratoplasty

Mark Draelos, Brenton Keller, Gao Tang, Anthony Kuo, MD, Kris Hauser, PhD, and Joseph Izatt, PhD

***Abstract*— Deep anterior lamellar keratoplasty (DALK) is a promising technique for corneal transplantation that avoids the chronic immunosuppression comorbidities and graft rejection risk associated with penetrating keratoplasty (PKP), the standard procedure. In DALK, surgeons must insert a needle 90 % through the 500 µm cornea without penetrating its underlying membrane. This pushes surgeons to their manipulation and visualization limits such that 59 % of DALK attempts fail due to corneal perforation or inadequate needle depth. We propose a robot-assisted solution to jointly solve the manipulation and visualization challenges using a cooperatively-controlled, precise robot arm and live optical coherence tomography (OCT) imaging, respectively. Our system features an interface handle, with which the surgeon and robot cooperatively hold the tool, and a posterior corneal boundary virtual fixture driven by real-time OCT segmentation. A study in which three operators performed DALK needle insertions manually and cooperatively in *ex vivo* human corneas demonstrated an 84 % improvement in perforation-free needle depth without an increased perforation rate.**

***Index Terms*— Cooperative control, medical robotics**

I. Introduction

Corneal transplants are among the most common allograft procedures performed worldwide. In the United States, nearly 40,000 full thickness corneal transplants, or penetrating keratoplasties (PKPs), are performed annually [1]. In the United Kingdom, corneal transplants outnumber kidney transplants by approximately 30 % each year [2]. Despite the success and widespread use of PKP, full thickness corneal transplants are not without drawbacks [3]. There is a substantial risk of immune rejection (35 % by year 10 post-surgery) which requires chronic, lifetime use of topical steroids with its side effects of glaucoma, cataracts, and infection [4]. The risk of complete graft failure (10–22 % by year 10) leads many who received their grafts before middle age to require a replacement graft later in life [4]. Furthermore, accidental trauma to the graft secured with fine sutures can rupture the eye and necessitate emergency repair and/or replacement.

An alternative form of corneal transplantation known as Deep Anterior Lamellar Keratoplasty (DALK) addresses many of PKP's drawbacks. In DALK, only the corneal epithelium and stroma are replaced, leaving the cellular and immunogenic host endothelium intact (Fig. 1). Because DALK preserves the endothelium, graft rejection is practically eliminated, and chronic immunosuppression is therefore unnecessary. The graft endothelium is also the predominant source of time-dependent graft failure; because the endothelium is not traumatized in DALK, graft failure is not accelerated as in PKP. Finally, as a technically extraocular procedure, the globe remains intact and is consequently less prone to rupture after trauma.

DALK's major barrier to adoption, however, is its great technical difficulty. In DALK, the surgeon must remove the top 90 % of the cornea (epithelium and stroma) while preserving the 10–20 µm endothelial layer complex underneath. This is currently accomplished via the "Big Bubble" technique wherein a needle is inserted into the cornea as close as possible to the endothelium without penetrating it (Fig. 1) [5]. Air is then injected to pneumo-dissect along the stromal-endothelial boundary (Descemet's membrane), forming a bubble that separates the stroma for excision. Inadvertently penetrating the endothelium terminates DALK and requires conversion to the usual PKP. Unfortunately, the Big Bubble technique requires extremely fine motor skills to reach the necessary depth without perforation and considerable experience to judge needle depth from a standard ophthalmic surgical microscope view (Fig. 2a–b). Even in experienced hands, 10 % of DALK procedures terminate in perforation, and 54 % of the remainder fail with poor

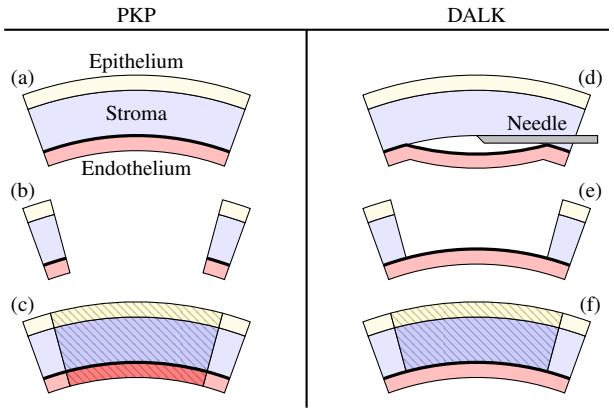

Fig. 1. (a) Corneal microanatomical structure showing epithelium (yellow), stroma (blue), Descemet's membrane (thick line), and endothelium (red) from top to bottom. Schematic drawing is not to scale. (a→c) PKP with full thickness corneal excision (b) and grafting (c). (d→f) DALK with needle insertion and bubble formation (d) followed by partial thickness corneal excision (e) and grafting (f).

*This research is partially supported by NIH F30-EY027280, NIH T32-GM007171, and the Coulter Translational Partnership.

M. Draelos, B. Keller, and J. Izatt are with the Department of Biomedical Engineering, Duke University, Durham, NC, USA. G. Tang is with the Department of Mechanical Engineering, Duke University, Durham, NC, USA. A. Kuo is with the Department of Ophthalmology, Duke University Medical Center, Durham, NC, USA. K. Hauser is with the Department of Electrical and Computer Engineering, Duke University, Durham, NC, USA. mark.draelos@duke.edu

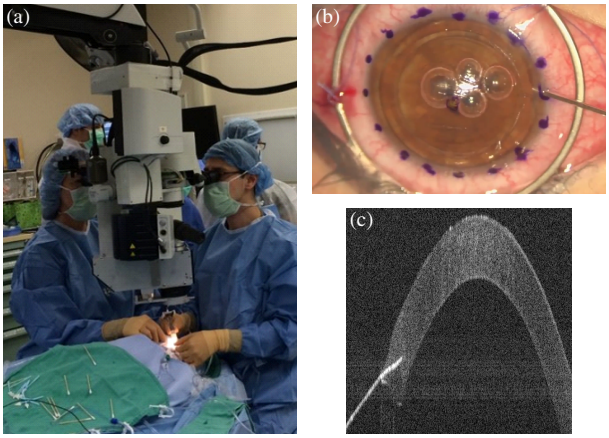

Fig. 2. (a) Microscope integrated OCT for visualization during ophthalmic procedures, adapted from [8] with permission. (b) DALK as viewed through an ophthalmic surgical microscope with limited ability to judge needle insertion depth, adapted from [9] under CC BY 3.0 license. (c) DALK as viewed using OCT with clearly resolved needle (white) and cornea (gray).

pneumo-dissection due to insufficient needle depth, yielding an overall failure rate of 59 % [6]. Surgeons need advances in both manipulation and visualization to reliably succeed at DALK.

We propose a cooperative robotic assistant with which surgeons can reliably complete DALK and thus avoid PKP's morbidities. The system combines a cooperatively-controlled, precise robot arm with live optical coherence tomography (OCT) imaging and anti-perforation virtual fixtures along the posterior corneal boundary (Fig. 2a,c). This assistant is most notable for equipping surgeons with stabilized hands and cross-sectional views needed to position a needle to $\pm 25\,\mu$m within the cornea. In this study of DALK needle insertions in *ex vivo* human corneas, operators using our system increased their corneal penetration depth by 32 % of corneal thickness, a key determinant of pneumo-dissection success [7], over manual insertions for perforation-free attempts.

II. Related Work

Ophthalmic microsurgery pushes surgeons to their physical limits. Surgeons not only must estimate depth using a top-down surgical microscope view but also must develop the manual dexterity to operate at microscopic scales. Even in routine procedures, surgeons face these visualization and manipulation hurdles. Technologies that advance ophthalmic microsurgery must address these challenges together.

From a visualization standpoint, optical coherence tomography (OCT) has emerged as a leading technology for ophthalmic visualization [8], [10]–[13]. In particular, microscope-integrated OCT (MIOCT) provides real-time cross-sectional and volumetric imaging without surgical interruptions. Despite finding considerable utility in both posterior and anterior segment surgery, OCT offers no support of manipulation. At best, surgeons can carefully guide their instruments. At worst, they can helplessly watch their tremor disturb the tool tip.

From a manipulation standpoint, several groups have explored hand stabilization and tremor reduction. The Steady Hand system uses cooperative control to attenuate tremor and implement virtual fixtures [14]–[16]. Its micrometer stage actuators are capable of very precise motions which the surgeon gains through the jointly held tool. The mechanical design, however, features a remote center of motion, which is disadvantageous for DALK's peripheral and shallow needle trajectories. Furthermore, the Steady Hand has a compact workspace that limits its flexibility for gross positioning of tools.

Similarly, the handheld Micron system uses internal miniature actuators to actively stabilize its needle tip and enforce virtual fixtures over a small distance [17]–[20]. It relies on an external visual tracking system to separate handle and needle motion. As a handheld robot, however, Micron cannot hold the tool independently, and, unlike a cooperative system, the surgeon must continuously maintain gross positioning. In addition, several teleoperation-based ophthalmic surgery system are under development, including those by PRECEYES [21], [22] and the ARMA group [23]. These systems target vitreoretinal surgery, and, despite their precision, are not well-suited to the shallow needle insertions found in DALK.

There is a clear vacuum where manipulation and visualization intersect in ophthalmic microsurgery. Systems that tightly couple fine manipulation and high-resolution visualization can fill that void and thereby enable surgeons with the technologies necessary to treat their patients.

III. Cooperative DALK Assistant

Our cooperative DALK assistant brings together a precision robot arm and high-resolution optical coherence tomography (OCT) imaging to overcome both manipulation and visualization challenges. Section III-A introduces the system's component parts while Sections III-B and III-C describe the signal and imaging processing, respectively, that drive the control system presented in Section III-D.

A. Hardware

The DALK assistant has two major hardware components: a robot arm with end-effector force sensing and an OCT system (Fig. 3a). The robot arm and the operator jointly manipulate the needle through an ergonomic "surgeon interface" handle (Fig. 3b). Both the handle-mounted needle and OCT scanner converge on the surgical site for real-time needle tracking (Fig. 3c). Together, these hardware components satisfy surgeons' manipulation and visualization needs during DALK.

Due to the fine precision needed when working with the 500 µm-thick cornea, we chose the IRB 120 robot arm (ABB Robotics; Zürich, Switzerland) for our system. This robot arm features 20 µm accuracy and 10 µm repeatability over a roughly $1\,\text{m}^3$ workspace and can therefore accomplish both gross positioning and fine tissue manipulation. With the IRB 120, we achieved sufficient precision for positioning a needle within 50 µm as needed in DALK while retaining the

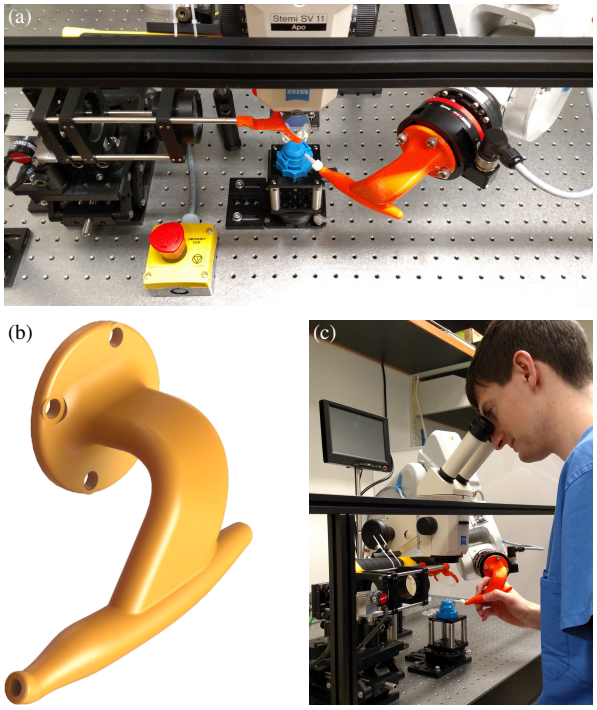

Fig. 3. (a) Cooperative DALK system, including robot arm (right), OCT scanner (left), microscope (center), and artificial anterior chamber (blue). (b) Ergonomic "surgeon interface" handle which affords a comfortable grip without causing mechanical interference at the surgical site. (c) Operator using the microscope to grossly position the needle tip before switching to OCT guidance.

flexibility of a general purpose arm. To provide cooperative interactions, we used a Gamma force-torque sensor (ATI Industrial Automation; Apex, NC) with ±32 N calibration for sensing at the surgeon interface.

For high-resolution imaging, we used a custom OCT engine built with a 100 kHz swept-source laser centered at 1050 nm (Axsun Technologies; Billerica, MA) and a telecentric scanner with a 15 cm working distance. The engine captured volumes with resolution $500 \times 128 \times 999$ voxels and field of view $12 \times 12 \times 5.5$ mm at 1.1 Hz. We chose these parameters to provide adequate sampling over the entire cornea. Custom C++ control and GPU-based OCT processing softwares provided real-time OCT visualization with ideal spatial resolution of $24 \times 94 \times 5.5$ µm. This imaging resolution provided the necessary visualization for monitoring needle insertions.

B. Force Signal Conditioning

The raw force-torque sensor signal required conditioning to eliminate measurement bias and gravity. Tool-induced static loads on the sensor during initialization induce a pose-dependent bias in later measurements that includes force ($\vec{f}_b$) and torque ($\vec{\tau}_b$) components.

$$\vec{f}_b = R_b^{-1} m\vec{g} \tag{1}$$

$$\vec{\tau}_b = \vec{a} \times \vec{f}_b, \tag{2}$$

where m and $\vec{a}$ are the tool mass and center-of-mass displacement from the measurement origin, respectively, R_b is the sensor pose in the world coordinate system when biased, and $\vec{g}$ is gravitational acceleration. Adding the bias to raw force ($\vec{f}_m$) and torque ($\vec{\tau}_m$) measurements eliminates it.

$$\vec{f} = R\left(\vec{f}_m + \vec{f}_b\right) \tag{3}$$

$$\vec{\tau} = R\left(\vec{\tau}_m + \vec{\tau}_b\right), \tag{4}$$

where $\vec{f}$ and $\vec{\tau}$ are the true force and torque, respectively, and R is the sensor pose for the measurement. When the sensor's pose is identical to its bias pose (i.e., $R = R_b$), the bias terms essentially restore tool-induced static loads. For cooperative control, gravity introduces undesirable forces and torques in sensor measurements. Subtracting the known tool static loads in the world coordinate system eliminates these effects to give the desired control force ($\vec{f}_c$) and torque ($\vec{\tau}_c$).

$$\vec{f}_c = \vec{f} - m\vec{g} \tag{5}$$

$$\vec{\tau}_c = \vec{\tau} - (R\vec{a}) \times (m\vec{g}) \tag{6}$$

Performing this conditioning, however, requires knowledge of R, R_b, m and $\vec{a}$. While R and R_b are generally well-known from robot forward kinematics and sensor mounting, m and $\vec{a}$ may vary with tool designs and changes (e.g., needle modifications). In such situations, m and $\vec{a}$ can be estimated with application of a known force and torque to the sensor. This is conveniently accomplished by subjecting the sensor to gravity alone (i.e., no external forces), yielding the following two equations with only m and $\vec{a}$ unknown.

$$\vec{f} = R\left(\vec{f}_m + R_b^{-1} m\vec{g}\right) = m\vec{g} \tag{7}$$

$$\vec{\tau} = R\left[\vec{\tau}_m + \vec{a} \times \left(R_b^{-1} m\vec{g}\right)\right] = (R\vec{a}) \times (m\vec{g}) \tag{8}$$

Rearrangement to isolate m and $\vec{a}$ gives

$$\vec{f}_m = \left(R^T - R_b^T\right) m\vec{g} = m\vec{u} \tag{9}$$

$$\vec{\tau}_m = \vec{a} \times \left[\left(R^T - R_b^T\right) m\vec{g}\right] = \vec{a} \times (m\vec{u}) \tag{10}$$

where

$$\vec{u} = \left(R^T - R_b^T\right) \vec{g} \tag{11}$$

is known. With raw force measurements ($\vec{f}_m$'s and $\vec{\tau}_m$'s) at different poses (R's), this gives a system of equations readily solved with non-linear optimization techniques (e.g., Nelder-Mead simplex) for m and $\vec{a}$ to calibrate the tool.

C. Cornea Segmentation and Needle Tracking

We provided OCT-based virtual fixtures to help prevent perforation using real-time corneal boundary segmentation and needle tracking at the OCT volume rate. We adapted previously described graph theory and dynamic programming approaches to corneal segmentation [24], [25] for real-time operation by overlapping with OCT volume acquisition and processing. For needle tracking, we incorporated a stepwise approach in [26] that identified tool A-scans in maximum intensity projections (MIPs) and then used iterative closest point [27] to fit a 3D needle model. MIP-based A-scan

identification exploited the needle's hyperreflectivity in OCT. Segmentation in B-scans with needle-obscured A-scans was corrected using image inpainting from [28].

D. Control System with Virtual Fixtures

The controller synthesized robot force sensing and OCT segmentation and needle tracking to provide stabilized cooperative robot-surgeon interactions and avoid corneal perforation. We chose a direct Cartesian force-velocity control law to guarantee no robot motion independent of surgeon-applied force.

$$\dot{\vec{q}} = J_o^{-1}(\vec{q}) \begin{bmatrix} RH & 0 \\ 0 & RH \end{bmatrix} G \begin{bmatrix} RH & 0 \\ 0 & RH \end{bmatrix}^T \begin{bmatrix} \vec{f}_c \\ \vec{\tau}_c \end{bmatrix}, \qquad (12)$$

where $\dot{\vec{q}}$ is the target joint velocity vector, $J_o(q)$ is the robot Jacobian about the tool center of rotation, H is the rotation matrix that defines the gain axes in the robot tool frame R, and G is the diagonal gain matrix. The surgeon thus remains in direct control of the needle at all times (i.e., $\vec{f}_c = \vec{\tau}_c = 0$ implies $\dot{\vec{q}} = 0$). For added usability, we provided a foot switch which held $\dot{\vec{q}} = 0$ until depressed. This allowed the surgeon to release the handle while maintaining needle position. We chose $G^{-1} = \mathrm{diag}(40, 40, 40, 0.9, 0.75, 0.4)$ in units of $\mathrm{N\,m^{-1}\,s}$ and $\mathrm{N\,m\,rad^{-1}\,s}$ to compensate for the surgeon interface handle's lever arms and discourage typically undesirable needle rotations during DALK (e.g., rotation in horizontal plane). Our control software (Fig. 4) provided dynamic gain adjustment (0–100 %) through a joystick throttle and operated with joint limits chosen to avoid singularities.

Using live corneal segmentation and needle tracking, the controller provided virtual fixtures to prevent perforation. After each OCT volume, the controller calculated the distance from the needle tip to the posterior corneal boundary. If that distance reduced below 50 µm (90 % of typical cornea thickness), the controller rejected control forces advancing or lowering the needle. This fixture remained active until the minimum observed distance exceeded the 50 µm threshold. For OCT volumes in which needle tracking failed, the controller maintained the prior fixture activation state.

We commanded the robot arm at 250 Hz through its Externally-Guided Motion interface, which offers 20 ms response time, using a custom C++ control software. We configured the robot controller for velocity-only tracking (zero position gain) and path low-pass filtering with 2 Hz bandwidth. This achieved highly responsive motion while rejecting oscillations from noise and control lag. Low-pass filtering also attenuated the operator's physiologic hand tremor.

IV. Methods

We designed a user study to compare DALK needle insertions performed manually (i.e., free-hand) and cooperatively with our system. Each operator completed training and testing needle insertion trials in *ex vivo* human corneas under Duke University Medical Center IRB approval. We simulated physiologic corneal conditions with a pressured artificial anterior chamber (Katena Products; Denville, NJ). For training,

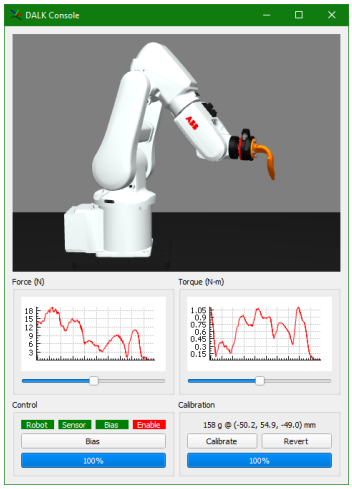

Fig. 4. Software console for robot interaction, providing control force-torque readouts, sensor biasing, and force control gain adjustment.

operators performed two sets of four consecutive manual and cooperative trials in a randomized order. Operators received verbal and video instruction on DALK technique, coaching on cooperative system operation, and OCT visualization of final needle depth for manual trials. For testing, operators performed eight trials alternating manual and cooperative with a randomized initial configuration. During manual trials, operators used a 27-gauge syringe-mounted needle with a 45° bend to perform needle insertions using only light microscope guidance, which replicated current surgical practice. During cooperative trials, operators used a 27-gauge robot-mounted needle to perform needle insertions using light microscope and real-time OCT guidance. Operators received no instruction or coaching once testing trials started.

For both training and testing, we asked operators to target 90 % needle depth at the corneal apex as is typical in surgical practice. Operators did not complete DALK with a pneumo-dissection to allow cornea reuse for eight trials. Operators used one cornea for training and another for testing. We rotated the cornea 45° after each trial to avoid reusing existing needle tracts and repressurized the artificial anterior chamber between trials at the operator's request. For cooperative trials, we adjusted the force control gain to 100 % during gross positioning, to 10 % during initial corneal penetration, and to 2 % during advancement to the corneal apex, relative to our baseline gain settings.

We recorded OCT volumes during the testing trials to evaluate for perforation and estimate final needle depth in later analysis. For this study, we defined perforation as clear evidence of needle penetration through the endothelial layer. A single grader blinded to the trial mode (manual or cooperative) reviewed each volume series for perforation and extracted the final needle depth. Using custom C++ software and the approach in [7], the grader extracted final needle depth from refraction-corrected OCT cross-sections as a percentage of corneal thickness along the top surface normal passing through the needle tip. The grader manually

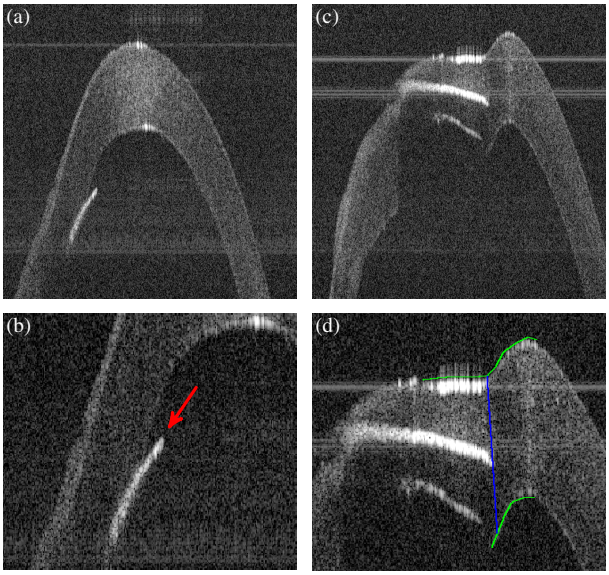

Fig. 5. Example OCT cross-sections illustrating (a–b) needle perforation into the anterior chamber (red arrow) and (c–d) final needle depth estimation with manual segmentation (green) and index-corrected surface normal (blue).

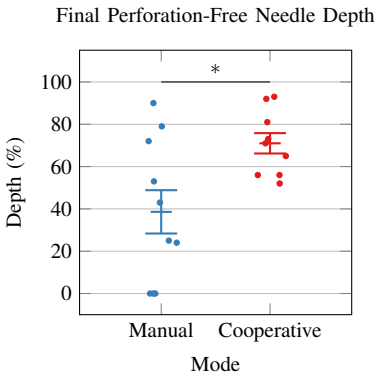

Fig. 6. Final perforation-free needle depth across all operators by mode. Improved performance is higher depth percentage. Each dot represents the depth of one perforation-free trial. Error bars indicate standard error of the mean. Asterisk denotes statistically significant difference.

segmented the corneal top and bottom boundaries for refraction correction and depth estimation purposes.

To compare manual and cooperative insertions, we analyzed the mean final needle depth and perforation rate by mode. We excluded trials with perforation from needle depth analysis rather than considering them "100 %" depth insertions. We assessed for statistical significance to the $p < 0.05$ level using ANOVA for needle depth and Fisher's exact test for perforation rate.

Additionally, we evaluated the IRB 120's repeatability using a 1 mil (25.4 µm) precision gage. We programmed the IRB 120 to repeatedly move throughout its workspace and then return to a fixed pose that depressed the gage's probe. We video recorded the gage's indicator during depression cycles at various program execution speeds. Furthermore, we measured OCT segmentation, needle tracking, and cooperative control latency during typical operating conditions by instrumenting our software.

V. Results

Three unaffiliated, volunteer operators performed a total of 24 DALK needle insertions across six corneas for evaluation. Two operators had no prior ophthalmic surgery experience whereas one operator had four years of ophthalmic surgery training without significant DALK exposure. Figure 5 shows representative examples of perforation and needle depth estimation from graded OCT volumes. Figure 6 shows the final needle depth for all perforation-free trials.

Operators inserted needles to a mean depth of 39 % manually and 71 % cooperatively. The 32 % of corneal thickness increase in mean depth from manual to cooperative trials was statistically significant ($F(1,13) = 6.7$, $p = 0.022$). There were no statistically significant differences in depth by operator ($F(2,13) = 0.02$, $p = 0.98$) or interactions between operator and mode ($F(2,13) = 1.7$, $p = 0.21$). The perforation rate was 2 of 12 (17 %) for manual trials and 3 of 12 (25 %) for cooperative trials. This difference was not statistically significant ($p = 1.0$).

We video recorded the gage indicator for 40 cycles of our IRB 120 repeatability test program. In all 40 cycles, the robot returned to the same pose to within one gage marking (25.4 µm). This yielded a repeatability no larger than 25.4 µm, although we were limited by the gage resolution. For OCT segmentation and needle tracking, we measured 150 ms of latency, yielding an overall 1.05 s delay for a complete volume. For cooperative control, we measured 60 ms of latency from sensed force to response motion.

VI. Discussion

With our cooperative system, operators nearly doubled their perforation-free mean needle insertion depth. This effect persisted across multiple operators, trials, and corneas. As a significant determiner of pneumo-dissection success [7], increasing mean needle insertion depth by 32 % of corneal thickness has large clinical ramifications. Depth of 39 % is associated with failed pneumo-dissection whereas depth of 71 % is associated with at least partial and likely full pneumo-dissection. This leads us to believe that the fine manipulation and high-resolution visualization our system offers can improve overall DALK success rates. The ultimate proof of success, however, is full pneumo-dissection which we did not evaluate to maximize trials per cornea.

Notably, our cooperative system did not significantly increase the perforation rate compared to manual trials in this study. The observed rates of 17 % and 25 % for manual and cooperative trials, respectively, are well within the previously reported range of 4–31.8 % [29]. Because the cooperative system decidedly changes the operator's haptic feedback during DALK by stabilizing the needle, one might expect increased perforations as the operator cannot directly sense their applied force. This is especially so when the force control gain is low, meaning that the robot's stiffness attenuates

any applied force. In contrast, we suspect that slowed needle movement during low force control gains allowed operators extra reaction time to avoid perforation.

Nevertheless, OCT segmentation and needle tracking latency posed a significant problem, as evidenced by cooperative perforations despite virtual fixtures. The 1.05 s lag in fixture updates certainly degraded their effectiveness. In fact, if the needle advanced faster than about $50\,\mu\mathrm{m\,s^{-1}}$, the fixture was unlikely to prevent perforation. This is most directly addressed by reducing the volume acquisition time, the largest contributor of latency, with faster swept-source lasers or less dense scan protocols. Furthermore, cooperatively limiting the needle insertion speed will make the fixtures more tolerant of delay.

VII. Conclusion

We have demonstrated an OCT-guided cooperative robot for improving needle insertion depth in an *ex vivo* human cornea DALK model. We believe this concept can improve DALK success rates and thereby spare patients the chronic immunosuppression comorbidities and graft rejection risk associated with PKP. In the future, we plan to incorporate needle path virtual fixtures via predictive modeling of corneal deformation to further reduce insertion depth variability.

References

[1] Eye Bank Association of America. (2017, April) 2016 Eye Banking Statistical Report.

[2] A. J. George and D. F. Larkin, "Corneal transplantation: the forgotten graft," *Am J Transplant*, vol. 4, no. 5, pp. 678–85, 2004.

[3] W. J. Reinhart, D. C. Musch, D. S. Jacobs, W. B. Lee, S. C. Kaufman, and R. M. Shtein, "Deep anterior lamellar keratoplasty as an alternative to penetrating keratoplasty a report by the american academy of ophthalmology," *Ophthalmology*, vol. 118, no. 1, pp. 209–18, 2011.

[4] S. P. Dunn, R. L. Gal, C. Kollman, D. Raghinaru, M. Dontchev, C. L. Blanton, E. J. Holland, J. H. Lass, K. R. Kenyon, M. J. Mannis, S. I. Mian, C. J. Rapuano, W. J. Stark, and R. W. Beck, "Corneal graft rejection 10 years after penetrating keratoplasty in the cornea donor study," *Cornea*, vol. 33, no. 10, pp. 1003–9, 2014.

[5] M. Anwar and K. D. Teichmann, "Big-bubble technique to bare Descemet's membrane in anterior lamellar keratoplasty," *J Cataract Refract Surg*, vol. 28, no. 3, pp. 398–403, 2002.

[6] V. M. Borderie, O. Sandali, J. Bullet, T. Gaujoux, O. Touzeau, and L. Laroche, "Long-term results of deep anterior lamellar versus penetrating keratoplasty," *Ophthalmology*, vol. 119, no. 2, pp. 249–55, 2012.

[7] N. D. Pasricha, C. Shieh, O. M. Carrasco-Zevallos, B. Keller, D. Cunefare, J. S. Mehta, S. Farsiu, J. A. Izatt, C. A. Toth, and A. N. Kuo, "Needle depth and big-bubble success in deep anterior lamellar keratoplasty: An ex vivo microscope-integrated OCT study," *Cornea*, vol. 35, no. 11, pp. 1471–1477, 2016.

[8] O. M. Carrasco-Zevallos, B. Keller, C. Viehland, L. Shen, G. Waterman, B. Todorich, C. Shieh, P. Hahn, S. Farsiu, A. N. Kuo, C. A. Toth, and J. A. Izatt, "Live volumetric (4D) visualization and guidance of in vivo human ophthalmic surgery with intraoperative optical coherence tomography," *Scientific Reports*, vol. 6, p. 31689, 2016.

[9] S. Luccarelli. (2017, May) SMALL BUBBLE DALK with Prof.BUSIN's Technique. University Eye Clinic of San Giuseppe Hospital. [Online]. Available: https://www.youtube.com/watch?v=uzLmS5XHZ2g

[10] Y. K. Tao, J. P. Ehlers, C. A. Toth, and J. A. Izatt, "Intraoperative spectral domain optical coherence tomography for vitreoretinal surgery," *Optics Letters*, vol. 35, no. 20, pp. 3315–7, 2010.

[11] O. M. Carrasco-Zevallos, B. Keller, C. Viehland, L. Shen, M. I. Seider, J. A. Izatt, and C. A. Toth, "Optical coherence tomography for retinal surgery: Perioperative analysis to real-time four-dimensional image-guided surgery," *Investigative Ophthalmology and Visual Science*, vol. 57, no. 9, pp. 37–50, Oct 2016.

[12] L. Shen, O. Carrasco-Zevallos, B. Keller, C. Viehland, G. Waterman, P. S. Hahn, A. N. Kuo, C. A. Toth, and J. A. Izatt, "Novel microscope-integrated stereoscopic heads-up display for intrasurgical optical coherence tomography," *Biomedical Optics Express*, vol. 7, no. 5, pp. 1711–26, 2016.

[13] C. Viehland, B. Keller, O. M. Carrasco-Zevallos, D. Nankivil, L. Shen, S. Mangalesh, T. Viet du, A. N. Kuo, C. A. Toth, and J. A. Izatt, "Enhanced volumetric visualization for real time 4D intraoperative ophthalmic swept-source OCT," *Biomedical Optics Express*, vol. 7, no. 5, pp. 1815–29, 2016.

[14] R. Taylor, P. Jensen, L. Whitcomb, A. Barnes, R. Kumar, D. Stoianovici, P. Gupta, Z. Wang, E. Dejuan, and L. Kavoussi, "A steady-hand robotic system for microsurgical augmentation," *The International Journal of Robotics Research*, vol. 18, no. 12, pp. 1201–1210, 1999.

[15] A. Üneri, M. A. Balicki, J. Handa, P. Gehlbach, R. H. Taylor, and I. Iordachita, "New steady-hand eye robot with micro-force sensing for vitreoretinal surgery," in *IEEE RAS/EMBS International Conference on Biomedical Robotics and Biomechatronics*, Sept 2010, pp. 814–819.

[16] R. Kumar, P. Jensen, and R. H. Taylor, "Experiments with a steady hand robot in constrained compliant motion and path following," in *IEEE International Workshop on Robot and Human Interaction (RO-MAN)*, 1999, pp. 92–97.

[17] C. N. Riviere, W. T. Ang, and P. K. Khosla, "Toward active tremor canceling in handheld microsurgical instruments," *IEEE Transactions on Robotics and Automation*, vol. 19, no. 5, pp. 793–800, 2003.

[18] W. T. Ang, C. N. Riviere, and P. K. Khosla, "Design and implementation of active error canceling in hand-held microsurgical instrument," in *IEEE/RSJ International Conference on Intelligent Robots and Systems (IROS)*, vol. 2, 2001, pp. 1106–1111.

[19] R. A. MacLachlan, B. C. Becker, J. C. Tabarés, G. W. Podnar, L. A. Lobes Jr, and C. N. Riviere, "Micron: an actively stabilized handheld tool for microsurgery," *IEEE Transactions on Robotics*, vol. 28, no. 1, pp. 195–212, 2012.

[20] B. C. Becker, R. A. MacLachlan, L. A. Lobes, G. D. Hager, and C. N. Riviere, "Vision-based control of a handheld surgical micromanipulator with virtual fixtures," *IEEE Transactions on Robotics*, vol. 29, no. 3, pp. 674–683, 2013.

[21] M. D. de Smet, S. H. Popma, G. Naus, T. H. C. M. Meenink, M. J. Beelen, and M. Steinbuch, "Robot-assisted choroidotomy and subretinal bleb creation," *Investigative Ophthalmology and Visual Science*, vol. 55, no. 13, pp. 2324–2324, 2014.

[22] M. D. de Smet, T. C. M. Meenink, T. Janssens, V. Vanheukelom, G. J. L. Naus, M. J. Beelen, C. Meers, B. Jonckx, and J.-M. Stassen, "Robotic assisted cannulation of occluded retinal veins," *PLOS ONE*, vol. 11, no. 9, pp. 1–16, Sept 2016.

[23] H. Yu, J.-H. Shen, K. M. Joos, and N. Simaan, "Design, calibration and preliminary testing of a robotic telemanipulator for OCT guided retinal surgery," in *IEEE International Conference on Robotics and Automation (ICRA)*, 2013, pp. 225–231.

[24] F. LaRocca, S. J. Chiu, R. P. McNabb, A. N. Kuo, J. A. Izatt, and S. Farsiu, "Robust automatic segmentation of corneal layer boundaries in sdoct images using graph theory and dynamic programming," *Biomedical Optics Express*, vol. 2, no. 6, pp. 1524–1538, 2011.

[25] S. J. Chiu, C. A. Toth, C. B. Rickman, J. A. Izatt, and S. Farsiu, "Automatic segmentation of closed-contour features in ophthalmic images using graph theory and dynamic programming," *Biomedical Optics Express*, vol. 3, no. 5, pp. 1127–1140, 2012.

[26] B. Keller, M. Draelos, G. Tang, S. Farsiu, A. N. Kuo, K. Hauser, and J. A. Izatt, "Real-time corneal segmentation and 3D surgical tool tracking in anterior segment intrasurgical OCT," *Biomedical Optics Express*, in preparation.

[27] P. J. Besl, N. D. McKay *et al.*, "A method for registration of 3-D shapes," *IEEE Transactions on Pattern Analysis and Machine Intelligence*, vol. 14, no. 2, pp. 239–256, 1992.

[28] M. Bertalmio, A. L. Bertozzi, and G. Sapiro, "Navier-stokes, fluid dynamics, and image and video inpainting," in *IEEE Computer Society Conference on Computer Vision and Pattern Recognition (CVPR)*, vol. 1, 2001, pp. I–355–I–362.

[29] M. Busin, V. Scorcia, P. Leon, and Y. Nahum, "Outcomes of air injection within 2mm inside a deep trephination for deep anterior lamellar keratoplasty in eyes with keratoconus," *American Journal of Ophthalmology*, vol. 164, no. Supplement C, pp. 6–13, 2016.